ACS APPLIED BIO MATERIALS

www.acsabm.org Article

Ag/ZnO/PMMA Nanocomposites for Efficient Water Reuse

Alessandro Di Mauro, Clayton Farrugia, Stephen Abela, Paul Refalo, Maurice Grech, Luciano Falqui, Giuseppe Nicotra, Gianfranco Sfuncia, Antonio Mio, Maria Antonietta Buccheri, Giancarlo Rappazzo, Maria Violetta Brundo, Elena Maria Scalisi, Roberta Pecoraro, Carmelo Iaria, Vittorio Privitera, and Giuliana Impellizzeri*

Cite This: *ACS Appl. Bio Mater.* 2020, 3, 4417−4426 Read Online

ACCESS | Metrics & More | Article Recommendations

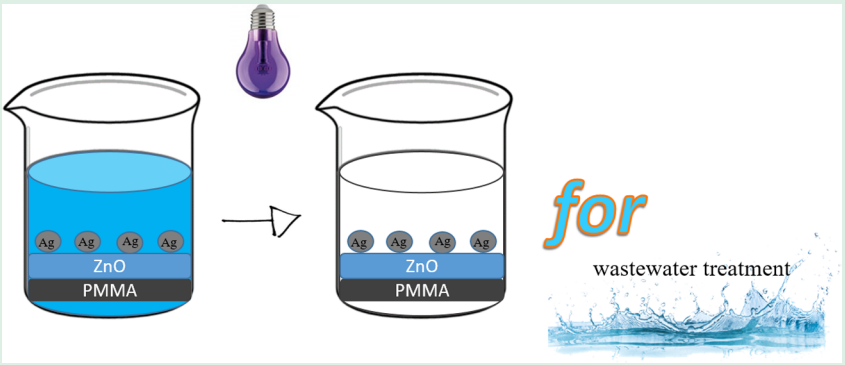

ABSTRACT: This work attempts to produce photocatalytic surfaces for large-scale applications by depositing nanostructured coatings on polymeric substrates. ZnO/poly(methyl methacrylate) (PMMA) composites were prepared by low-temperature atomic layer deposition (ALD) of ZnO on PMMA substrates. In addition, to increase the photocatalytic and antibacterial activities of ZnO films, Ag nanoparticles were added on ZnO surfaces using plasma-enhanced ALD. The morphology, crystallinity, and chemical composition of the specimens were meticulously examined by scanning and transmission electron microscopies, energy-dispersive X-ray spectroscopy, and X-ray diffraction analyses. The noteworthy photocatalytic activity of the nanocomposites was proved by the degradation of the following organic pollutants in aqueous solution: methylene blue, paracetamol, and sodium lauryl sulfate. The antibacterial properties of the samples were tested using *Escherichia coli* as a model organism. Moreover, the possible toxic effects of the specimens were checked by biological tests. The present results unambiguously indicate the Ag/ZnO/PMMA nanocomposite as a powerful tool for an advanced wastewater treatment technology.

KEYWORDS: *silver, ZnO, polymer, ALD, low temperature, photocatalysis, water*

INTRODUCTION

The World Health Organization estimated that by 2025 half of the world's population will reside in areas with high water-stress.[1] An improvement of water supply and sanitation, and a better management of water resources, especially in terms of water reuse, can greatly contribute to poverty reduction and can boost economic growth in low-income countries.

Conventional technologies of water treatment, such as sedimentation, adsorption, and filtration, simply transfer the contaminants from one medium to another one, without destroying the pollutants. In addition, some of these methodologies, such as inverse osmosis, have high operating and energetic costs. Consequently, it is crucial to find new strategies to recycle wastewater efficiently, in a low-cost and eco-friendly manner. This would contribute to the mitigation of the water scarcity problem.

Heterogeneous photocatalysis is one of the emergent and innovative methods for wastewater treatment. The rationale of this process is based on the production of highly reactive species (i.e., $OH^{\bullet}$, $O_2^{\bullet-}$) active in the mineralization of organic contaminants and water pathogens (see as examples refs 2−8). In brief, when a semiconductor photocatalyst immersed in polluted water is irradiated by photons with an energy equal to or higher than its band-gap energy, the produced electron−hole pairs can cause the generation of reactive oxygen species

Received: April 14, 2020
Accepted: June 22, 2020
Published: June 22, 2020

https://dx.doi.org/10.1021/acsabm.0c00409
ACS Appl. Bio Mater. 2020, 3, 4417−4426

(ROSs) on the photocatalyst surfaces. The ROSs promote oxidation processes, which destroy organic compounds and damage microorganisms possibly present in water. Photocatalysis can be seen as a definitive and eco-friendly approach for the degradation of contaminants and reduction of bacteria load from wastewater.

A limiting factor of semiconductor photocatalysts is that the photoexcited electrons in the conduction band quickly recombine with the holes in the valence band, with dissipation of energy. This is an undesired effect since it lowers the efficiency of the photocatalytic process. Therefore, the addition of electron scavengers is decisive for lengthening the recombination time of charge carriers and thereby improving the photocatalytic performance. The coupling with noble metal (e.g., Ag, Au, Pt) nanoparticles can be used for enhancing the charge separation. Noble metals with a Fermi level lower than the conduction band level of the semiconductor photocatalyst induce a Schottky junction at the metal/semiconductor interface. The photoexcited electrons can be effectively trapped by the metals, increasing as a consequence the separation of the electrons and holes.[6,9,10]

Nowadays, one of the major technological obstacles hindering the commercialization of photocatalysts is the recovery of the photocatalytic powders after the wastewater treatment. Photocatalysts in the powder form are highly efficient due to their high surface areas; however, nanoparticles can be extremely toxic to aquatic and human lives,[11] and a laborious separation process is required prior to their reuse and the discharge of the treated water. The incorporation/anchoring of active nanomaterials in a polymeric matrix is a promising strategy to solve this problem. Polymeric nanocomposites have recently attracted great attention in the research community because they possess flexibility, formability, low weight, and low costs.[12−18] However, the low softening/melting temperatures of polymers are an obstacle for the synthesis of hybrid materials composed of an inorganic part. Indeed, semiconductor photocatalysts and noble metals are conventionally prepared by physical or chemical vapor deposition (CVD) methods at substrate/reactor temperatures higher than 200 °C.[19−23] Such temperatures are incompatible with the thermally fragile polymers. The authors have already reported on the atomic layer deposition (ALD) of ZnO photocatalytic films at low deposition temperatures (from 40 to 120 °C).[24,25] The atomic layer deposition technique is a chemical vapor deposition process, used for manufacturing conformal inorganic material films with thickness down to the fraction of a nanometer.[26,27] The benefits of ALD compared to other CVD processes stem from the use of self-terminating surface reactions, which induce the formation of uniform, homogeneous, conformal, and reproducible films over complex substrates.[26,27] ALD at low temperatures has been particularly chosen as the deposition technique for the production of the materials presented in this work.

In this article, the authors report on hybrid nanomaterials consisting of poly(methyl methacrylate) (PMMA) as the base material, ZnO layers, and Ag nanoparticles. PMMA is an ordinary polymeric material, used in numerous applications for its transparency to visible light, chemical stability, mechanical properties, and low cost. For these reasons, it is a viable matrix material for the realization of photocatalytic nanocomposites.[15,17,25,28] ZnO has been chosen for its great photocatalytic activity under UV light irradiation, easy growth, low cost, and low environmental impact.[25,29,30] The noble metal Ag has been used as an electron scavenger as explained above but also for its antibacterial properties.[31] The ZnO films and the Ag nanoparticles have been laid on the PMMA substrates using ALD at low deposition temperatures. The authors have already reported the deposition of ZnO on PMMA substrates by low-temperature ALD.[25] Atomic layer deposition of Ag has been demonstrated, but to date, not that at low temperature.[32−36] Despite countless applications of silver in antimicrobial surfaces, sensors, catalysis, microelectronics, decorative coatings, reflective surfaces, and others, the deposition of Ag using ALD is still at an initial phase of development.[32−36] The first paper reporting the thin-film deposition of Ag by ALD dates back to 2007,[36] while the first article describing the ALD deposition of Ag nanoparticles was published in 2010.[35] Prof. M. Leskelää's group originally studied the plasma-enhanced−atomic layer deposition (PE-ALD) of thin silver films on silicon and soda lime glass. In their investigation, Ag(fod)-(PEt_3) was used as a silver precursor held in plasma-activated hydrogen, with growth temperatures of 120−150 °C.[34] A more recent work reports the large-scale deposition of silver nanoparticles on 8 in. Si wafers using PE-ALD and temperatures between 120 and 160 °C.[32] So the authors performed a meticulous study to optimize the PE-ALD of silver at low temperatures. After detailed morphological, structural, and chemical characterizations, the hybrid nanomaterials were tested for the photocatalytic degradation of methylene blue (MB), paracetamol, and sodium lauryl sulfate (SDS) and for their antibacterial activity, too. The possible toxicity of the specimens was estimated by the zebrafish embryo toxicity test (ZFET), in agreement with the Organization for Economic Co-operation and Development (OECD).[37]

EXPERIMENTAL SECTION

Materials. Silicon wafers 8 in., (100)-oriented, purchased from Si-Mat, and 4 mm thick plates of PMMA synthetized by Plastica Alfa using the polymeric injection molding method, were employed as substrates for the ALD deposition processes. Diethyl zinc (DEZ), bought from Air Liquide, and Ag(fod)(PEt_3) ((fod = 2,2-dimethyl-6,6,7,7,8,8,8-heptafluorooctane-3,5-dionato), triethylphosphine-(6,6,7,7,8,8,8-heptafluoro-2,2-dimethyl-3,5-octanedionate)silver(I)) purchased from STREM, were used as ALD precursors for the deposition of ZnO and Ag, respectively. Methylene blue, paracetamol, and sodium lauryl sulfate were bought from Sigma-Aldrich and utilized as received for the photocatalytic tests. The *Escherichia coli* ATCC25922 strain was used as a model organism for the bacterial tests. Fertilized zebrafish eggs (wild-type) were provided by the Center of Experimental Ichthyiopathology of Sicily (CISS) of the University of Messina (Italy).

Preparation. Depositions of ZnO and Ag were performed employing Picosun R-200 ALD advanced equipment, provided with remote plasma too. Flat substrates of Si and PMMA, each measuring 2.5 × 2.5 cm^2, were used. Deposition on PMMA was carried out at 80 °C, a temperature compatible with the PMMA polymer. In the case of Si substrates, the deposition was at 155 °C (in addition to 80 °C). PMMA substrates were first washed in a solution of deionized water and isopropanol and then dried under nitrogen flux. Silicon substrates were used as received.

Zinc oxide depositions were thermally performed, keeping the chamber temperature at 80 or 155 °C. The ZnO layers were obtained using DEZ (purity ≥ 99.9999%) and deionized water as precursors and N_2 (purity ≥ 99.999%) as carrier and purge gas. The pulse and purge times were set at 0.1, 3.0, 0.1, and 5.0 s for DEZ, N_2, H_2O, and N_2, respectively. The temperature of the precursors was kept at 22 °C.

The silver depositions were performed on ZnO layers, through plasma-enhanced ALD (PE-ALD). The plasma was created with capacitive coupling using an rf power source of 13.56 MHz. The

https://dx.doi.org/10.1021/acsabm.0c00409
ACS Appl. Bio Mater. 2020, 3, 4417−4426

power of the plasma was 2800 W. A mixture of hydrogen (3%) and helium (97%) was used for the activation of the plasma. The gas mixture (purity ≥ 99.999%) was blended with argon (purity ≥ 99.999%) to guarantee plasma ignition. The hydrogen/helium flux was fixed at 120 sccm, while the argon plasma gas flux was 50 sccm. The silver precursor, Ag(fod)(PEt_3), was placed onto a bottle and vaporized at 75 or 147 °C. During silver depositions, the chamber temperature was fixed at 80 or 155 °C, respectively. The pulse length of the metal precursor was 4 s, while the pulse length of the plasma was 14 s. The purge length after the metal precursor was 6 s, while that after the exposure of the plasma was 4 s.

Characterizations. The thickness of the ZnO layers was measured using a Woollam M-2000 spectroscopic ellipsometer.

The surface morphology of the synthesized materials was investigated using a field emission Zeiss Supra 25 scanning electron microscopy (SEM), operating at 3 kV, and supplied with an Oxford solid-state detector for energy-dispersive X-ray spectroscopy (EDS). Prior to analyses, the samples deposited on PMMA were coated with a 3 nm thick gold film using sputter deposition. The coating made the surfaces conductive, preventing the charging of the electron beam by the insulating and polymeric substrate.

A comprehensive scanning transmission electron microscopy (STEM) investigation was carried out with a JEOL ARM200-F Cs-corrected microscope, supplied with a cold-field emission gun having an energy spread of 0.3 eV and operating at 200 keV. The probe size was 0.7 Å at 200 kV. In a conventional TEM (CTEM) mode, micrographs are acquired in the bright field (BF), while in the STEM mode, imaging can also be performed in the Z-contrast mode using high-angle annular dark field (HAADF). During sample rastering, a Centurio energy-dispersive spectrometer (EDS) by Gatan, equipped with a 100 mm^2 silicon drift detector, was used for the simultaneous STEM-EDS acquisition.

The structure of the specimens was studied through a Bruker D-500 X-ray diffractometer (XRD), with a parallel Cu Kα radiation operating at 40 kV, 40 mA, 2θ in the range of 20−60°, and the grazing incidence mode (0.8°). The XRD patterns were analyzed by the Bruker software suite, containing the Inorganic Crystal Structure Database (ICSD) structure database.

Photocatalytic Tests. The photocatalytic activity of the nanocomposites under investigation was first tested for the degradation of methylene blue dye in deionized water, under UV light irradiation. A UWAVE LED UV lamp system, with an emission centered at 365 nm (full width at half-maximum of 10 nm) and an irradiance of 12 mW/cm^2, was employed as the light source. Before taking any measurements, the specimens were illuminated by the UV lamp for 60 min to eliminate the hydrocarbons from the surface of the specimens.[38] The samples were afterward dipped in a 4 mL solution consisting of MB at an initial concentration of 1.5×10^{-5} M and deionized water. Before switching on the UV light, the solution was held in the dark for 1 h to assess the adsorption of the MB by the beaker and sample surfaces. The solution was then irradiated again, and the absorbance of the solution was measured at regular time intervals for a period of up to 4 h, using a ultraviolet−visible (UV−vis) spectrophotometer (Lambda 45, PerkinElmer) with a scan range of 200−800 nm. The decomposition of MB was estimated by measuring the absorbance of the 664 nm peak in the Lambert−Beer regime.[39] The degradation of MB dye in the absence of any photocatalysts served as the control.

The samples were also analyzed for the decomposition of paracetamol, one of the most popular analgesic and antipyretic drugs. The test was carried out with the same method reported above for MB photodegradation. The initial solution contained paracetamol, with a concentration of 1.5×10^{-5} M, in deionized water. The degradation of paracetamol was estimated by following the absorbance peak at 243 nm in the Lambert−Beer regime.[39]

The photocatalytic activity of the synthesized samples was also investigated for the degradation of sodium lauryl sulfate, a surfactant frequently used in many cleaning and personal hygiene products for its foaming effect. SDS degradation was tested after 4 h of UV irradiation using a visible spectrophotometer (Hach DR 3900) and the LCK 432 cuvette kits for high-concentration solutions and LCK 332 cuvette kits for low-concentration solutions. The starting concentration of SDS was set at 4.3 mg/L (1.5×10^{-5} M).

The experimental error of the photocatalytic measurements was 1%.

Bacterial Tests. Antibacterial activity was checked on the *Escherichia coli (E. coli)* ATCC25922 strain. Bacteria were regularly maintained through spreading on McConkey agar plates. Inocula were prepared starting by a single colony plunged in 30 mL of Luria−Bertani broth and grown overnight at 37 °C. The broth was agitated constantly at 180 rpm under aerobic conditions. The following morning, the bacterial growth was measured by optical density at 600 nm. Bacteria were diluted up to 10^6 CFU/mL in phosphate-buffered saline (PBS), and 200 μL was added onto the photocatalyst specimens. A humid chamber was realized, according to the ISO standard 27447:2019,[40] and samples were covered with a quartz glass to avoid drying during irradiation. A UV lamp, centered at 368 nm, with a full width at half-maximum lower than 10 nm, and with an irradiance of 1.1 mW/cm^2, was used to induce photocatalysis (as required by the ISO standard 27447:2009).[40] Bacteria exposed only to UV light were treated in parallel as controls. After a 1 h exposure, bacteria were recovered, opportunely diluted by serial dilutions 1:10, and plated in Luria−Bertani agar Petri dishes that were incubated overnight at 37 °C. CFUs were counted the following morning. The results were normalized toward the "substrate"-only sample and plotted as percentages. The experimental error was around 5%. Experiments were repeated three times.

Zebrafish Embryo Toxicity (ZFET) Test. The ZFET test was carried out in agreement with the Organization for Economic Co-operation and Development (OECD).[37] Bloodstock zebrafish, reared at the Center of Experimental Ichthyiopathology of Sicily (CISS) husbandry, were maintained in a standalone unit (Tecniplast) under controlled environmental conditions, as reported by refs 41, 42. The fertilized eggs used for the test were selected according to ref 43. To evaluate the potential toxic effects of the samples, healthy embryos were placed in a 100 mL glass beaker (20 embryos in 30 mL of deionized water) and kept for 96 h postfertilization together with the synthetized materials. The embryonic/larval mortality and hatching rate were estimated every 24 h. Each experiment was repeated three times. During the exposure period, the embryos were photographed with a stereomicroscope (Leica M0205C, Multifocus). Five larvae from each group were selected for immunodetection of biomarkers, according to ref 43. Observations were performed employing a fluorescence microscope (NIKON ECLIPSE Ci), equipped with a NIKON DS-Qi2 camera.

RESULTS AND DISCUSSION

A preliminary study was performed to optimize the PE-ALD of silver. The experiment was carried out using silicon substrates, since Si resists higher temperatures. To facilitate the deposition of the metal, a thin layer of ZnO was always deposited prior to the deposition of Ag. The ZnO films were obtained as reported in the Experimental Section. The pulse and purge times were set at 0.1, 3.0, 0.1, and 5.0 s for DEZ, N_2, H_2O, and N_2, respectively, and a total of 50 cycles was applied. In the PE-ALD of Ag, 600 cycles were used and the deposition temperature was varied. The earliest Ag deposition was achieved with a precursor temperature of 147 °C and a chamber temperature of 155 °C, to ensure a high concentration of precursor in the deposition chamber. Figure 1a reports a SEM in top-view of a deposited surface. The morphology of silver deposited at 155 °C appears as an aggregation of Ag nanoparticles. Since the objective was to use PMMA as substrates, the subsequent depositions were performed at a precursor temperature of 75 °C and a chamber temperature of 80 °C, which is below the glass-transition temperature of the PMMA (~100 °C). Figure 1b displays the

https://dx.doi.org/10.1021/acsabm.0c00409
ACS Appl. Bio Mater. 2020, 3, 4417−4426

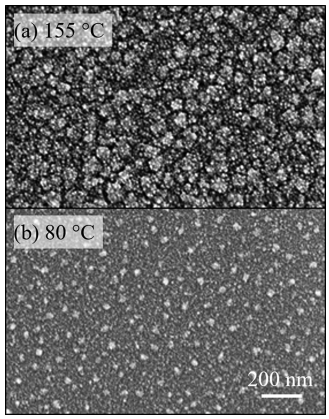

Figure 1. SEM images, in plan-view, of Ag nanoparticles on ZnO deposited on Si using PE-ALD at (a) 155 °C and (b) 80 °C after 600 cycles.

surface morphology of Ag deposited at 80 °C. The silver nanoparticles appear smaller and sparser compared to those deposited at 155 °C (Figure 1a). The observed trend of silver particle coalescence at higher temperature is expected and is in good agreement with that published in ref 35.

Once the deposition temperature of Ag was set at 80 °C, the authors studied the effect of changing the number of cycles from 600 to 75. With the aim of analyzing the samples by cross-view CTEM, the materials were arranged by standard mechanical polishing followed by low-energy Ar^+ ion milling, using a Gatan PIPSII system. Figure 2 presents several TEM

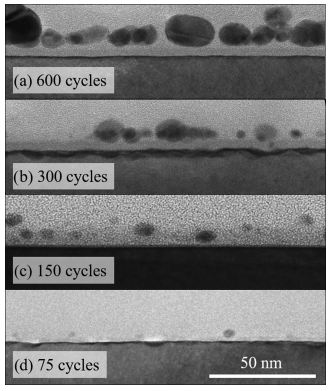

Figure 2. TEM images, in cross view, of Ag nanoparticles deposited on ZnO coatings and Si substrates using PE-ALD at 80 °C and varying cycles: (a) 600, (b) 300, (c) 150, and (d) 75.

cross-sectional images of Ag deposited at 80 °C on a ~4 nm layer of ZnO, deposited on the Si substrate. The dimension of Ag nanoparticles was estimated from the TEM images. The Ag nanoparticles are almost spherical in shape. The silver obtained after 600 cycles (Figure 2a) appears as a discontinuous film composed of silver nanoparticles of 10−25 nm in diameter. The largest particles are formed by the agglomeration of several nanoparticles. As the number of cycles used decreases, a decrease in particle size is observed. Deposition after 300 cycles (Figure 2b) shows nanoparticles with a size between 4 and 15 nm. Even in this case, some agglomeration is still evident. Deposition after 150 cycles (Figure 2c) shows a further reduction of particle size and an increase in distance between nanoparticles. Lastly, the samples synthetized using 75 cycles (Figure 2d) exhibit few nanoparticles with a mean size of about 4 nm.

For the purpose of evaluating the impact of the ALD cycles on the photoactivity of the synthetized materials, the degradation of methylene blue under UV light irradiation was assessed. Figure 3 shows the change of MB concentration

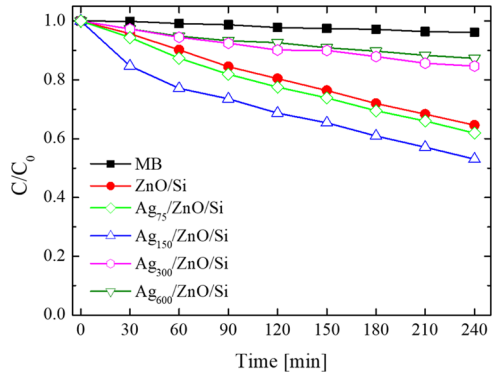

Figure 3. Variation of MB as a function of the irradiation time for MB with no sample (filled squares), MB with a sample containing a ZnO film (filled circles), MB with a sample containing a ZnO film and Ag nanoparticles after 75 cycles (open diamonds), 150 cycles (open triangles), 300 cycles (open circles) and 600 cycles (open inverted triangles).

with irradiation time. The concentration of MB at time t is denoted as C and at time zero as C_0. As expected, in the absence of a photocatalyst, no degradation of MB was observed (filled squares in Figure 3). Only the samples deposited using 150 cycles (open triangles in Figure 3) showed an appreciable increment in the photocatalytic activity with respect to the ZnO reference samples (filled circles in Figure 3). In this case, an increase of about 20% was recorded. The samples deposited after 75 cycles (open diamonds in Figure 3) did not show any appreciable variation of the photocatalytic activity, probably because the quantity of silver is too little to enhance the photocatalytic effect. On the other hand, specimens obtained following 300 cycles (open circles) and 600 cycles (inverted open triangles) manifested a decrease of ca. 35% in the photocatalytic capacity. This is probably due to a lower surface area of ZnO in contact with the polluted water. In this case, the silver nanoparticles shielded the ZnO layers.

To quantitatively confront the photocatalytic activity of the nanocomposites, the Langmuir−Hinshelwood model can be applied assuming a first-order degradation mechanism.[6] In this case, the reaction rate constant (k) is given by the subsequent equation

$$\ln \frac{C_0}{C} = kt \tag{1}$$

where t is the irradiation time. The rate constants were consequently determined by the linear interpolation of the relationship 1 seen before.[44] The obtained values of the rate constants are displayed in Table 1. The values shown in Table 1 are in compliance with the recently reported rate constant values of similar systems,[45] considering the different nature of the nanostructuring of the materials.

Once the Ag deposition on ZnO was optimized in terms of the deposition temperature (suitable for the PMMA) and the number of cycles (maximizing the photocatalysis), then the whole deposition process (i.e., Ag and ZnO) was applied to the

https://dx.doi.org/10.1021/acsabm.0c00409
ACS Appl. Bio Mater. 2020, 3, 4417−4426

Table 1. Values of Rate Constants for MB Photodegradation

sample	rate constant (min^{-1})
MB	$1.7 \pm 0.2 \times 10^{-5}$
ZnO/Si	$1.8 \pm 0.3 \times 10^{-3}$
Ag_{75}/ZnO/Si	$2.0 \pm 0.1 \times 10^{-3}$
Ag_{150}/ZnO/Si	$2.8 \pm 0.4 \times 10^{-3}$
Ag_{300}/ZnO/Si	$7.3 \pm 0.1 \times 10^{-4}$
Ag_{600}/ZnO/Si	$6.1 \pm 0.4 \times 10^{-4}$

PMMA substrates. The authors have already reported the depositions of ZnO on plastic substrates.[15,24,25] In detail, we synthetized several thin layers of ZnO on Si substrates using the low-temperature ALD technique (between 40 and 120 °C). All of the ZnO layers were polycrystalline, despite the low temperature. The films deposited at 80 °C revealed the best photocatalytic performances, due to the crystallographic orientation of the films. Then, the deposition process was transferred on flexible substrates: poly(ethylene naphthalate) (PEN)[24] and PMMA.[15,25] In the present work, the authors deposited ZnO on PMMA substrates using the optimized recipe (0.1, 3.0, 0.1, and 5.0 s for DEZ, N_2, H_2O, and N_2, respectively) and a total of 1650 cycles. The high number of cycles led to the formation of ZnO flat films, 100 ± 7 nm in thickness (as measured by ellipsometry) with significant photocatalytic efficiency. The authors then deposited Ag nanoparticles on top of the ZnO films, using PE-ALD, a chamber temperature of 80 °C, and 150 cycles. Figure 4

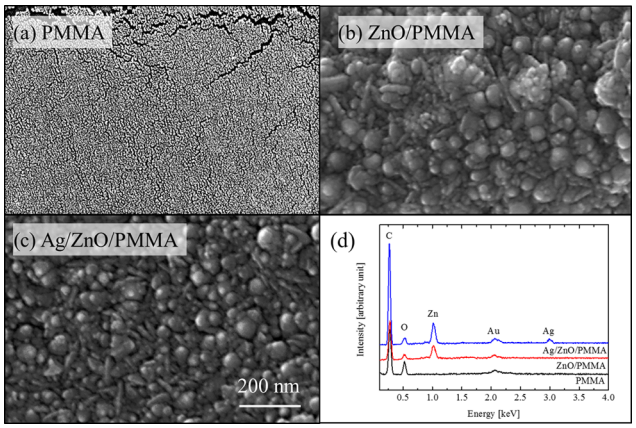

Figure 4. SEM images, in plan-view, of (a) PMMA, (b) ZnO/PMMA, (c) Ag/ZnO/PMMA, and (d) EDS patterns of the surfaces investigated.

displays the morphological and structural results obtained for Ag and ZnO depositions on PMMA. All of the samples were sputtered with a thin film of gold to carry out the SEM analyses. The PMMA substrates (Figure 4a) showed the morphology of the gold layer together with the cracks typical of polymers. The samples deposited with ZnO (Figure 4b) displayed a granular morphology typical of ZnO.[24,25,46] The surface morphology was not significantly modified by the addition of Ag (the reader can compare Figure 4b,c). The surface morphology of the Ag/ZnO/PMMA samples is different from the Ag/ZnO/Si counterpart surface (compare Figure 4c with 1b). This is thought to be due to the different interaction of the zinc precursor with the polymer and the Si substrates. The EDS analysis of the Ag/ZnO/PMMA samples shows the presence of silver at 2.98 eV (Figure 4d). Silver is not present in the other samples.

Figure 5 shows the diffractograms of PMMA-based samples. The PMMA substrates having no surface deposits only show a

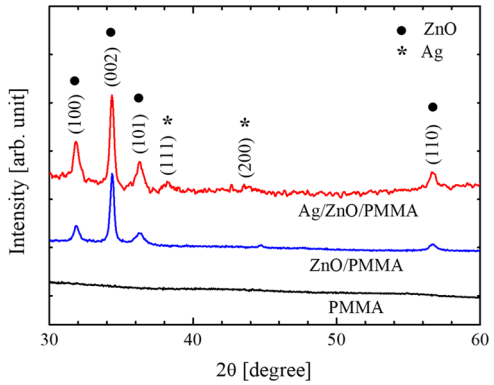

Figure 5. XRD patterns of PMMA, ZnO/PMMA, and Ag/ZnO/PMMA samples.

broad band at about 30° typical of amorphous materials. In comparison, the PMMA samples deposited with ZnO display peaks corresponding to the crystallographic planes of the ZnO in the wurtzite structure, namely, the (100), (002), (101), and (110) planes at 31.9, 34.4, 36.3, and 56.7°, respectively. The samples enriched with Ag show additional reflections at 2θ values of 38.2 and 44.3°. These correlate to the (111) and (200) reflections of the face-centered cubic Ag structure. The weak intensity of the diffraction features can be ascribed to the small size and low density of the Ag nanoparticles.

A detailed study of Ag nanoparticles deposited on ZnO/PMMA was performed using a probe-corrected STEM microscope in plan-view. Prior to starting the analyses, the PMMA substrate was removed to avoid the charge accumulation due to the electron beam and the insulating nature of the PMMA, which would otherwise result in image blurring and/or loss of contrast during imaging. The PMMA was dissolved in acetone after having capped the surface of the sample with a supporting layer of conductive-epoxy resin, necessary to maintain the mechanical strength of the Ag/ZnO layer. Multilayers of epoxy resin were built on the Ag/ZnO surface followed by final mechanical thinning in preparation for specimen plan-view observation. The results are summarized in Figure 6. Figure 6a is a plan-view BF-STEM image, showing

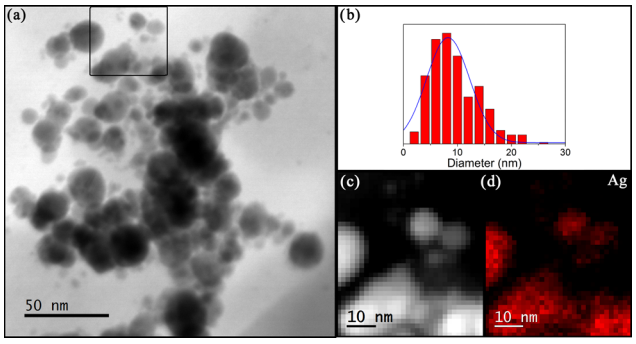

Figure 6. (a) BF-STEM image of Ag nanoparticles. (b) Diameter distribution of Ag nanoparticles fitted with a Gaussian distribution curve (blue line). STEM spectrum imaging analysis: (c) HAADF signal is shown in grayscale and (d) Ag EDS signal is reported in red.

https://dx.doi.org/10.1021/acsabm.0c00409
ACS Appl. Bio Mater. 2020, 3, 4417−4426

the Ag nanoparticles supported by the ZnO substrate. As seen earlier and as displayed in Figure 2, the largest Ag particles are assembled by agglomeration of several nanoparticles. Figure 6b displays the diameter distribution of the Ag nanoparticles. These values fitted the Gaussian distribution (blue line) with a peak at 8.0 ± 0.6 nm. A detailed chemical analysis was performed by the electron beam scanning pixel-by-pixel over the region enclosed by the black square in Figure 6a. The corresponding Z-contrast STEM-HAADF signal and the EDS spectra were acquired in a data cube and then are represented in two-dimensional (2D) maps reported in Figure 6c and d, respectively. Particularly, in Figure 6d, only the photon counts acquired from individual pixels and pertaining to the Ag EDS signal were collected and used to create the 2D chemical map. From the plots, it is now easy to see that the black particles in Figure 6a, corresponding to the bright region of the Z-contrast HAADF image of Figure 6c, and the red regions in the EDS 2D chemical map displayed in Figure 6d are indeed Ag nanoparticles.

The photocatalytic capability of the samples deposited on PMMA was first investigated for the degradation of MB dye under the UV lamp system. Figure 7 reports the variation in

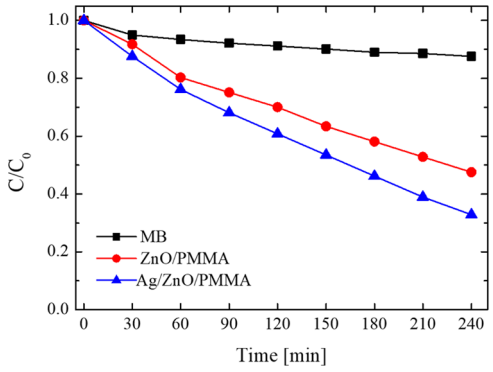

Figure 7. Degradation of MB dye as a function of the irradiation time for MB and no catalyst (squares), MB with ZnO/PMMA (circles), and MB with Ag/ZnO/PMMA (triangles) samples.

concentration of MB with irradiation time. Testing of the photoactivity of the coated PMMA specimens started by evaluating the degradation of MB under UV light and with no catalyst. The test was carried out as a reference and is shown by square plot symbols in Figure 7. The samples enriched with Ag nanoparticles manifested an increase of about 30% in photocatalytic capacity over the ZnO/PMMA counterpart samples (compare the plot with triangles to that with circles in Figure 7). This enhanced capability is ascribed to the ability of the metal to prolong the recombination time of the charge carriers.[6]

The comparison in performance between samples with a Si base (Figure 3) and those having a polymer substrate (Figure 7) is of interest. It is evident that plastic systems have improved efficiency. The biggest difference was observed for the ZnO pure layers. This phenomenon can be related to the different thicknesses of ZnO deposited on PMMA (~100 nm) and that on Si (~4 nm) substrates. In 2016, the authors published that the photocatalytic efficiency of ZnO ALD films improves with film thickness until they reach saturation at about 50 nm.[24] The increase in photoactivity with thickness is a result of increased volume and consequently more charge carriers created by photoabsorption. With increased thickness however, the charge carriers in-depth recombine before reaching the surface, thus explaining why saturation is reached. That said, we cannot exclude an additional effect due to the different substrates (i.e., PMMA and Si) on the photoactivity of the specimens.

The synthetized nanocomposites were also checked for the degradation of new-generation contaminants, such as pharmaceuticals. The authors chose to test paracetamol because it is one of the most commonly used drugs worldwide. Figure 8

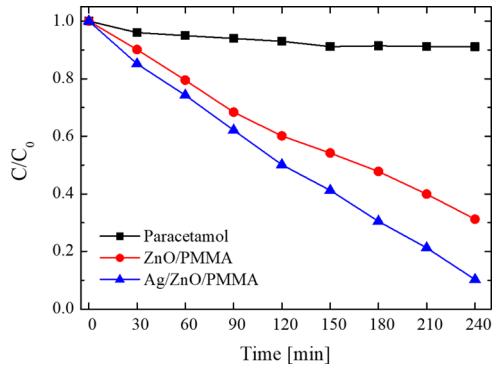

Figure 8. Degradation of paracetamol drug as a function of irradiation time for paracetamol alone (squares), paracetamol with ZnO/PMMA (circles), and paracetamol with Ag/ZnO/PMMA (triangles) samples.

reports the degradation of paracetamol as a function of the UV irradiation time. The test was carried out with the same procedure used for MB photodegradation (reported in the Experimental Section). The concentration of paracetamol without any photocatalytic materials was reported as a reference (squares in Figure 8). The synthetized materials and in particular Ag/ZnO/PMMA samples are especially effective in degrading paracetamol (triangles in Figure 8). Indeed, after 4 h of irradiation, 90% paracetamol was degraded. The presence of Ag nanoparticles on the sample surface improves the photocatalytic activity by about 65% with respect to the ZnO samples (compare curves with triangles with that having circles in Figure 8). This is induced by the electron-scavenger effect of the metal nanoparticles.[6]

Particular attention is being paid to the treatment of greywater, i.e., all of the wastewater generated in households or office buildings including that from hand basins, showers, baths, washing machines, and dishwashers excluding black water contamination. Since one of the main contaminants in greywater is from anionic surfactants, the authors investigated the effects of the synthetized photocatalysts on sodium lauryl sulfate. The experimental results, after 4 h of UV light irradiation, are reported in Figure 9. The Ag/ZnO/PMMA samples showed a great aptitude in photodegrading the SDS surfactant. In fact, more than 90% of SDS was eliminated.

The rate constants for the photodegradation of MB, paracetamol, and SDS by the different samples are reported in Table 2.

The significant increase in the photodegradation rate constants observed in the samples decorated with Ag nanoparticles is due to the effect of the noble metal.[6] Figure 10 shows the mechanisms involved. When ZnO is exposed to UV light, the electrons of the semiconductor move from the valence band to the conduction band. Since the Fermi level of Ag is lower

https://dx.doi.org/10.1021/acsabm.0c00409
ACS Appl. Bio Mater. 2020, 3, 4417−4426

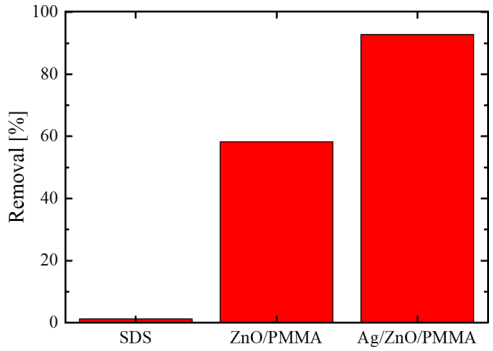

Figure 9. Degradation of sodium lauryl sulfate after 4 h of UV light irradiation for SDS alone, SDS with ZnO/PMMA, and SDS with Ag/ZnO/PMMA samples.

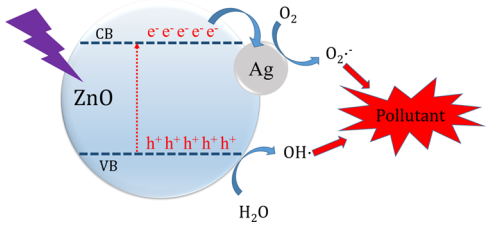

Figure 10. Electron capture by Ag nanoparticles in contact with ZnO.

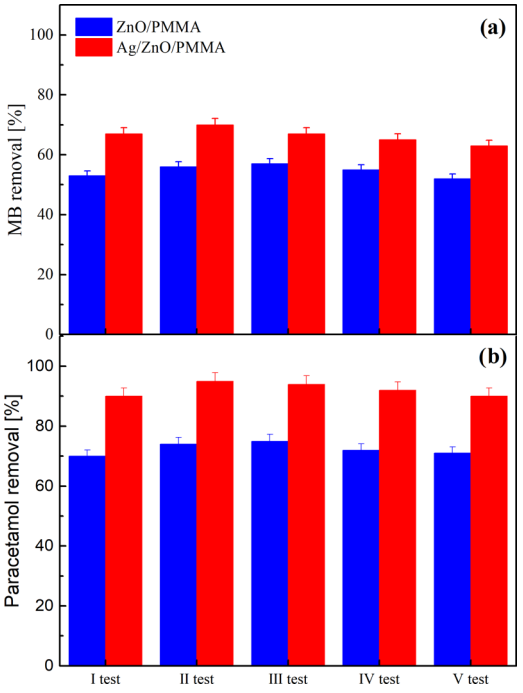

Figure 11. Recyclability of ZnO/PMMA and Ag/ZnO/PMMA samples after five tests of (a) MB and (b) paracetamol photodegradation.

than that of ZnO, the photoexcited electrons can move from the conduction band of the ZnO to the metal nanoparticles deposited on the ZnO surface. The oxygen molecules dissolved in water, being an electronic acceptor, capture the electrons and convert them into superoxide radicals. Furthermore, the holes of the ZnO, created when electrons are excited in the conduction band, induce the generation of hydroxyl radicals. The free radicals are efficiently involved in the photocatalytic oxidation of the pollutants. The metal, acting as an electron sink, reduces the probability of electron−hole recombination, implicating an effective charge separation and great photocatalytic reaction rates. Thus, the Ag nanoparticles lead to the observed higher photocatalytic activity.

It is worth noting that the synthetized nanocomposites are more effective in the degradation of paracetamol drug and SDS surfactant than MB dyes (the reader can compare Figures 8, 9, and 7 and consider Table 2). This data can be correlated to the electrostatic interaction between the ZnO layers and the different pollutants. Indeed, the ZnO positive surface would preferentially adsorb negative-charged pollutants, such as paracetamol and SDS.

The nanocomposites were tested up to five times to verify the recyclability of the synthetized samples. In detail, the recyclability tests were performed with MB and paracetamol for 4 h of UV light irradiation. At the end of each test, the samples were rinsed and left in deionized water for 2 h under UV light irradiation to take away possible remains of pollutants. The recyclability test is reported in Figure 11. Figure 11a refers to the experiment with the MB, while Figure 11b refers to the experiment with the paracetamol. Both types of samples, i.e., ZnO/PMMA and Ag/ZnO/PMMA, exhibited great stability in the photodegradation of the selected pollutants, demonstrating the reusability of the synthetized nanocomposites.

The photocatalytic capacity of the synthetized nanomaterials was also tested under visible-light irradiation for the degradation of MB. The experiment, performed by an Oriel VeraSol-2 solar simulator with ZnO/PMMA and Ag/ZnO/PMMA samples, did not reveal any aptitude of the nanocomposites in the degradation of the dye under solar light.

The antibacterial properties of the hybrid materials were checked by measuring the survival rate of *E. coli* after exposure to the samples synthetized. Experiments were run both under UV irradiation and in the dark, to estimate the photocatalytic contribution to the displayed antibacterial activity. Figure 12 shows that, after 60 min exposure to the ZnO/PMMA samples under UV illumination, ca. 40% of the exposed bacteria were still surviving, while in the dark, the surviving bacteria were about 95% This antibacterial effect can be ascribed to the photocatalytic activation of ZnO layers. Samples decorated with Ag nanoparticles performed far better than the ZnO/PMMA ones. In fact, after 60 min, the level of surviving bacteria was reduced to 0%. Tests run in the dark indicated that the antibacterial capacity is mostly due to the

Table 2. Values of the Rate Constants for MB, Paracetamol, and SDS Photodegradation

	rate constant (min^{-1})		
sample	MB	paracetamol	SDS
without catalyst	$1.7 \pm 0.2 \times 10^{-5}$	$4.9 \pm 0.2 \times 10^{-4}$	$6.0 \pm 0.1 \times 10^{-5}$
ZnO/PMMA	$3.1 \pm 0.2 \times 10^{-3}$	$4.4 \pm 0.1 \times 10^{-3}$	$3.5 \pm 0.2 \times 10^{-3}$
Ag/ZnO/PMMA	$4.4 \pm 0.3 \times 10^{-3}$	$7.5 \pm 0.2 \times 10^{-3}$	$1.0 \pm 0.1 \times 10^{-2}$

https://dx.doi.org/10.1021/acsabm.0c00409
ACS Appl. Bio Mater. 2020, 3, 4417−4426

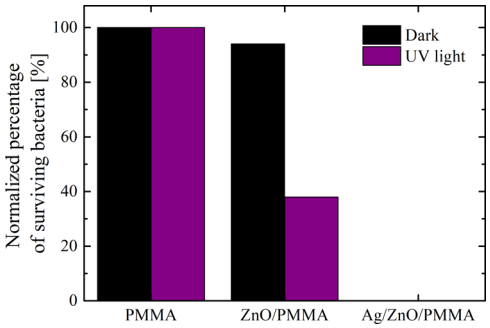

Figure 12. Normalized percentage of surviving *E. coli* bacteria in the dark and when exposed to UV irradiation in contact with PMMA, ZnO/PMMA, and Ag/ZnO/PMMA samples.

antimicrobial properties of silver, as results did not change whether samples are under UV illumination or in the dark.

The results of photocatalytic and bacteriological tests demonstrate the potential of the Ag/ZnO/PMMA composites for use in an efficient water recycling system.

In view of real application, checking the possible toxicity of the proposed nanomaterial is essential. To this end, the authors investigated the material's toxicity through zebrafish as the animal model. ZFET is a useful acute toxicity test recommended by the European Commission and aimed to reduce the impact of experiments on live animals. In fact, the use of zebrafish as an animal model has been suggested in several toxicology studies because it is a cheap, quick, and easy model to determine the toxicity of nanocompounds.[43,47] The ZFET test evaluates different endpoints: viability, growth (larval length), brain morphology, other craniofacial structures, heart, fins, notochord, somites, tail, body shape, cardiovascular function, yolk sac, locomotor function, and touch response. The experiment revealed that PMMA, ZnO/PMMA, and Ag/ZnO/PMMA samples cause neither mortality nor sublethal effects. Figure 13 is a microscope image of a zebrafish larvae after being in contact with a Ag/ZnO/PMMA sample for 48 h.

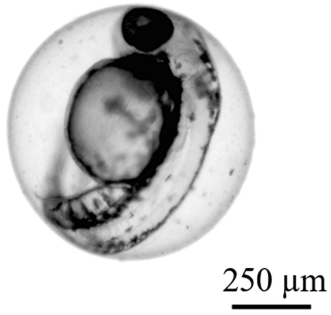

Figure 13. Zebrafish larvae after 48 h postfertilization treatment by exposure to Ag/ZnO/PMMA samples.

The untreated larvae and the larvae exposed to three types of nanomaterials (PMMA, ZnO/PMMA, and Ag/ZnO/PMMA) showed the expression of anti-MTs 1 antibody only in the head region (Figure 14). This biological response of the larvae allows us to exclude the toxicity of the examined materials.[48]

CONCLUSIONS

In conclusion, the authors presented the synthesis of a new hybrid nanomaterial incorporating a PMMA polymer, ZnO films, and Ag nanoparticles. The ZnO thin films and Ag nanoparticles were both deposited on PMMA substrates using ALD at low temperatures. The addition of Ag nanoparticles significantly improved the photocatalytic activity of pure ZnO and was able to degrade several organic contaminants such as methylene blue dye, paracetamol drug, and sodium lauryl sulfate surfactant. The observed enhancement of the photocatalysis is due to the decrease of the electron−hole recombination, thanks to the electron-scavenger effect of the metal. Concerning the antibacterial activity of the samples investigated, the materials enriched with Ag nanoparticles were able to kill completely all of the *E. coli* bacteria, even without any contribution of the ZnO photocatalyst. The safety of the nanocomposites was established using the zebrafish embryo toxicity test. This work lays the foundations for applications in hybrid composite devices based on PMMA and suitable for purifying wastewater for efficient reuse. The scaling-up required is expected to be relatively easy.

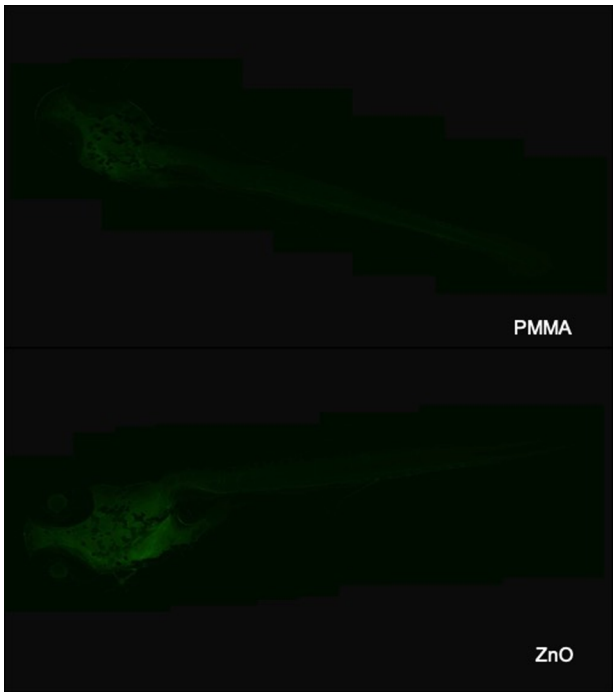

Figure 14. Zebrafish larvae after 96 h postfertilization treatment by exposure to Ag/ZnO/PMMA and treated with anti-MTs-1 antibody (green).

AUTHOR INFORMATION

Corresponding Author

Giuliana Impellizzeri − *CNR-IMM, 95123 Catania, Italy;*
orcid.org/0000-0002-1402-6346;
Email: giuliana.impellizzeri@ct.infn.it

Authors

Alessandro Di Mauro − *CNR-IMM, 95123 Catania, Italy;*
orcid.org/0000-0002-0534-0907

Clayton Farrugia − *Department of Metallurgy & Materials Engineering, Faculty of Engineering, University of Malta, Msida MSD 2080, Malta*

Stephen Abela − *Department of Metallurgy & Materials Engineering, Faculty of Engineering, University of Malta, Msida MSD 2080, Malta*

https://dx.doi.org/10.1021/acsabm.0c00409
ACS Appl. Bio Mater. 2020, 3, 4417−4426

Paul Refalo − *Department of Industrial & Manufacturing Engineering, Faculty of Engineering, University of Malta, Msida MSD 2080, Malta*
Maurice Grech − *Department of Metallurgy & Materials Engineering, Faculty of Engineering, University of Malta, Msida MSD 2080, Malta*
Luciano Falqui − *Plastica Alfa SpA, C. da Santa Maria Poggiarelli, 95041 Caltagirone (CT), Italy*
Giuseppe Nicotra − *CNR-IMM, 95121 Catania, Italy*
Gianfranco Sfuncia − *CNR-IMM, 95121 Catania, Italy*
Antonio Mio − *CNR-IMM, 95121 Catania, Italy*
Maria Antonietta Buccheri − *Department of Biological, Geological and Environmental Science, University of Catania, 95124 Catania, Italy*
Giancarlo Rappazzo − *Department of Biological, Geological and Environmental Science, University of Catania, 95124 Catania, Italy*
Maria Violetta Brundo − *Department of Biological, Geological and Environmental Science, University of Catania, 95124 Catania, Italy*
Elena Maria Scalisi − *Department of Biological, Geological and Environmental Science, University of Catania, 95124 Catania, Italy*
Roberta Pecoraro − *Department of Biological, Geological and Environmental Science, University of Catania, 95124 Catania, Italy*
Carmelo Iaria − *Department of Chemical, Biological, Pharmacological and Environmental Science, University of Messina, 98166 Messina, Italy*
Vittorio Privitera − *CNR-IMM, 95123 Catania, Italy*

Complete contact information is available at: https://pubs.acs.org/10.1021/acsabm.0c00409

Author Contributions

A.D.M. and G.I. conceived the idea; L.F. provided the PMMA substrates; A.D.M. performed the ALD, the SEM analyses, and the photocatalytic tests; C.F., S.A., and P.R. provided the XRD measurements; G.N., G.S., and A.M. carried out the TEM investigations; M.A.B. and G.R. provided the bacteriological tests; M.V.B., E.M.S., R.P., and C.I. performed the ecotoxicity studies; V.P. and M.G. reviewed and commented on the manuscript at all stages; and G.I. and A.D.M. interpreted the experimental data and wrote the manuscript. All authors read the manuscript and approved the final version.

Funding

This work was funded by the Interreg V. A. Italia-Malta (FESR) "Micro WatTS" project (CUP: B61G18000070009). The TEM analyses were performed at Beyond-Nano laboratory of the CNR-IMM, which is supported by the Italian Ministry of Education and Research (MIUR) under the "Beyond-Nano" project (PON a3_00363). The toxicity tests were supported by the PON project "AIM" founded by the European Social Found (CUP: E66C18001300007).

Notes

The authors declare no competing financial interest.

■ ACKNOWLEDGMENTS

The authors wish to thank Giuseppe Pantè (CNR-IMM) and James Camilleri (University of Malta) for technical assistance. The authors are grateful to Stefania Stefani (University of Catania) for the *E. coli* strain.

■ REFERENCES

(1) https://www.who.int/news-room/fact-sheets/detail/drinking-water.
(2) Shen, S.; Kronawitter, C.; Kiriakidis, G. An overview of photocatalytic materials. *J. Materiomics* **2017**, *3*, 1−2.
(3) Li, X.; Yu, J.; Jaroniec, M. Hierarchical photocatalysis. *Chem. Soc. Rev.* **2016**, *45*, 2603−2636.
(4) Scuderi, V.; Buccheri, M. A.; Impellizzeri, G.; Di Mauro, A.; Rappazzo, G.; Bergum, K.; Svensson, B. G.; Privitera, V. Photocatalytic and antibacterial properties of titanium dioxide flat film. *Mater. Sci. Semicond. Process.* **2016**, *42*, 32−35.
(5) Impellizzeri, G.; Scuderi, V.; Romano, L.; Napolitani, E.; Sanz, R.; Carles, R.; Privitera, V. C ion-implanted TiO_2 thin film for photocatalytic applications. *J. Appl. Phys.* **2015**, *117*, No. 105308.
(6) Chong, M. N.; Jin, B.; Chow, C. W. K.; Saint, C. Recent developments in photocatalytic water treatment technology: A review. *Water Res.* **2010**, *44*, 2997−3027.
(7) Gaya, U. I.; Abdullah, A. H. Heterogeneous photocatalytic degradation of organic contaminants over titanium dioxide: A review of fundamentals, progress and problem. *J. Photochem. Photobiol., C* **2008**, *9*, 1−12.
(8) Fujishima, A.; Rao, T. N.; Tryk, D. A. Titanium dioxide photocatalysis. *J. Photochem. Photobiol., C* **2000**, *1*, 1−21.
(9) Di Mauro, A.; Zimbone, M.; Scuderi, M.; Nicotra, G.; Fragalà, M. E.; Impellizzeri, G. Effect of Pt nanoparticles on the photocatalytic activity of ZnO nanofibers. *Nanoscale Res. Lett.* **2015**, *10*, No. 484.
(10) Scuderi, V.; Impellizzeri, G.; Romano, L.; Scuderi, M.; Brundo, M. V.; Bergum, K.; Zimbone, M.; Sanz, R.; Buccheri, M. A.; Simone, F.; Nicotra, G.; Svensson, B. G.; Grimaldi, M. G.; Privitera, V. An enhanced photocatalytic response of nanometric TiO_2 wrapping of Au nanoparticles for eco-friendly water applications. *Nanoscale* **2014**, *6*, 11189−11195.
(11) Li, Q.; Mahendra, S.; Lyon, D. Y.; Brunet, L.; Liga, M. V.; Li, D.; Alvarez, P. J. Antimicrobial nanomaterials for water disinfection and microbial control: Potential applications and implications. *Water Res.* **2008**, *42*, 4591−4602.
(12) Ussia, M.; Di Mauro, A.; Mecca, T.; Cunsolo, F.; Nicotra, G.; Spinella, C.; Cerruti, P.; Impellizzeri, G.; Privitera, V.; Carroccio, S. C. ZnO-pHEMA nanocomposites: An ecofriendly and reusable material for water remediation. *ACS Appl. Mater. Interfaces* **2018**, *10*, 40100−40110.
(13) Pellegrino, G.; Carroccio, S. C.; Ruffino, F.; Condorelli, G. G.; Nicotra, G.; Privitera, V.; Impellizzeri, G. Polimeric platform for the growth of chemically anchored ZnO nanostructures by ALD. *RSC Adv.* **2018**, *8*, 521−530.
(14) Srikanth, B.; Goutham, R.; Badri, N. R.; Ramprasath, A.; Gopinath, K. P.; Sankaranarayanan, A. R. Recent advancements in supporting materials for immobilised photocatalytic applications in waste water treatment. *J. Environ. Manage.* **2017**, *200*, 60−78.
(15) Di Mauro, A.; Cantarella, M.; Nicotra, G.; Pellegrino, G.; Gulino, A.; Brundo, M. V.; Privitera, V.; Impellizzeri, G. Novel synthesis of ZnO/PMMA nanocomposites for photocatalytic applications. *Sci. Rep.* **2017**, *7*, No. 40895.
(16) Sanz, R.; Buccheri, M. A.; Zimbone, M.; Scuderi, V.; Amiard, G.; Impellizzeri, G.; Romano, L.; Privitera, V. Photoactive layered nanocomposites obtained by direct transferring of anodic TiO_2 nanotubes to commodity thermoplastics. *Appl. Surf. Sci.* **2017**, *399*, 451−462.
(17) Cantarella, M.; Sanz, R.; Buccheri, M. A.; Ruffino, F.; Rappazzo, G.; Scalese, S.; Impellizzeri, G.; Romano, L.; Privitera, V. Immobilization of nanomaterials in PMMA composites for photocatalytic removal of dyes, phenols and bacteria from water. *J. Photochem. Photobiol., A* **2016**, *321*, 1−11.
(18) Schwartz, V. B.; Thétiot, F.; Ritz, S.; Pütz, S.; Choritz, L.; Lappas, A.; Förch, R.; Landfester, K.; Jonas, U. Antibacterial surface coatings from zinc oxide nanoparticles embedded in poly(*N*-isopropylacrylamide) hydrogel surface layers. *Adv. Funct. Mater.* **2012**, *22*, 2376−2386.

(19) Barreca, D.; Comini, E.; Ferrucci, A. P.; Gasparotto, A.; Maccato, C.; Maragno, C.; Sberveglieri, G.; Tondello, E. First example of ZnO-TiO_2 nanocomposites by chemical vapor deposition: Structure, morphology, composition, and gas sensing performances. *Chem. Mater.* **2007**, *19*, 5642−5649.
(20) Barreca, D.; Gasparotto, A.; Maccato, C.; Maragno, C.; Tondello, E. TiO_2 thin films by chemical vapor deposition: An XPS characterization. *Surf. Sci. Spectra* **2007**, *14*, 27−33.
(21) Gao, L.; Härter, P.; Linsmeier, Ch.; Wiltner, A.; Emling, R.; Schmitt-Landsiedel, D. Silver metal organic chemical vapour deposition for advanced silver metallization. *Microelectron. Eng.* **2005**, *82*, 296−300.
(22) Gao, L.; Härter, P.; Linsmeier, C.; Gstöttner, J.; Emling, R.; Schmitt-Landsiedel, D. Metalorganic chemical vapour deposition of silver thin films for future interconnects by direct liquid injection system. *Mater. Sci. Semicond. Process.* **2004**, *7*, 331−335.
(23) Yuan, Z.; Dryden, N. H.; Vittal, J. J. R.; Puddephatt, J. Chemical vapour deposition of silver. *Chem. Mater.* **1995**, *7*, 1696−1702.
(24) Di Mauro, A.; Cantarella, M.; Nicotra, G.; Privitera, V.; Impellizzeri, G. Low temperature atomic layer deposition of ZnO: Applications in photocatalysis. *Appl. Catal., B* **2016**, *196*, 68−76.
(25) Di Mauro, A.; Fragalà, M. E.; Privitera, V.; Impellizzeri, G. Review, ZnO for application in photocatalysis: From thin films to nanostructures. *Mater. Sci. Semicond. Process.* **2017**, *69*, 44−51.
(26) *Atomic Layer Deposition of Nanostructured Materials*, Pinna, N.; Knez, M., Eds.; Wiley-VCH: Weinheim, Germany, 2012.
(27) George, S. M. Atomic layer deposition: An overview. *Chem. Rev.* **2010**, *110*, 111−131.
(28) Demir, M. M.; Memesa, M.; Castignolles, P.; Wagner, G. PMMA/Zinc Oxide nanocomposites prepared by *in-situ* bulk polymerization. *Macromol. Rapid Commun.* **2006**, *27*, 763−770.
(29) Lee, K. M.; Lai, C. W.; Ngai, K. S.; Juan, J. C. Recent developments of zinc oxide based photocatalyst in water treatment technology: A review. *Water Res.* **2016**, *88*, 428−448.
(30) Cantarella, M.; Di Mauro, A.; Gulino, A.; Spitaleri, L.; Nicotra, G.; Privitera, V.; Impellizzeri, G. Selective degradation of paracetamol by molecularly imprinted ZnO nanonuts. *Appl. Catal., B* **2018**, *238*, 509−517.
(31) Piedade, A. P.; Vieira, M. T.; Martins, A.; Silva, F. *In vitro* behaviour of nanocrystalline silver-sputtered thin films. *Nanotechnology* **2007**, *18*, No. 105103.
(32) Wack, S.; Popa, P. L.; Adjeroud, N.; Guillot, J.; Pistillo, B. R.; Leturcq, R. Large-scale deposition and growth mechanism of silver nanoparticles by plasma-enhanced atomic layer deposition. *J. Phys. Chem. C* **2019**, *123*, 27196−27206.
(33) Hämäläinen, J.; Ritala, M.; Leskelä, M. Atomic layer deposition of noble metals and their oxides. *Chem. Mater.* **2014**, *26*, 786−801.
(34) Kariniemi, M.; Niinistö, J.; Hatanpää, T.; Kemell, M.; Sajavaara, T.; Ritala, M.; Leskelä, M. Plasma-enhanced atomic layer deposition of silver thin films. *Chem Mater.* **2011**, *23*, 2901−2907.
(35) Chalker, P. R.; Romani, S.; Marshall, P. A.; Rosseinsky, M. J.; Rushworth, S.; Williams, P. A. Liquid injection atomic layer deposition of silver nanoparticles. *Nanotechnology* **2010**, *21*, No. 405602.
(36) Niskanen, A.; Hatanpää, T.; Arstila, K.; Leskelä, M.; Ritala, M. Radical-enhanced atomic layer deposition of silver thin films using phosphine-adducted silver carboxylates. *Chem. Vap. Deposition* **2007**, *13*, 408−413.
(37) OECD. *Guideline for the Testing of Chemicals Fish Embryo Toxicity (FET) test*; OECD: Paris, 2013.
(38) Wang, R.; Hashimoto, K.; Fujishima, A.; Chikuni, M.; Kojima, E.; Kitamura, A.; Shimohigoshi, M.; Watanabe, T. Light-induced amphiphilic surfaces. *Nature* **1997**, *388*, 431−432.
(39) McNaught, A. D.; Wilkinson, A. *Compendium of Chemical Terminology*, 2nd ed.; Blackwell Scientific Publications: Oxford, 1997.
(40) *ISO 27447:2019, Fine ceramics (advanced ceramics, advanced technical ceramics) - Test method for antibacterial activity of semiconducting photocatalytic.*
(41) Iaria, C.; Saoca, C.; Guerrera, M. C.; Ciulli, S.; Brundo, M. V.; Piccione, G.; Lanteri, G. Occurrence of diseases in fish used for experimental research. *Lab. Anim.* **2019**, *53*, 619−629.
(42) Iaria, C.; Migliore, S.; Macri, D.; Bivona, M.; Capparucci, F.; Gaglio, G.; Marino, F. Evidence of *Centrocestus formosanus* (Nishigori, 1924) in Zebrafish (*Danio rerio*). *Zebrafish* **2019**, *16*, 522−526.
(43) Fiorenza, R.; Di Mauro, A.; Cantarella, M.; Iaria, C.; Scalisi, E. M.; Brundo, M. V.; Gulino, A.; Spitaleri, L.; Nicotra, G.; Dattilo, S.; Carroccio, S. C.; Privitera, V.; Impellizzeri, G. Preferential removal of pesticides from water by molecular imprinting on TiO_2 photocatalysts. *Chem. Eng.* **2020**, *379*, No. 122309.
(44) Melinte, V.; Stroea, L.; Buruiana, T.; Chibac, A. L. Photocrosslinked hybrid composites with Ag, Au or Au-Ag NPs as visible light triggered photocatalysts for degradation/reduction of aromatic nitroderivatives. *Eur. Polym. J.* **2019**, *121*, No. 109289.
(45) Din, M. I.; Khalid, R.; Hussain, Z. Minireview: Silver-doped titanium dioxide and silver-doped zinc oxide photocatalysts. *Anal. Lett.* **2018**, *51*, 892−907.
(46) Guziewicz, E.; Kowalik, I. A.; Godlewski, M.; Kopalko, K.; Osinniy, V.; Wójcik, A.; Yatsunenko, S.; Łusakowska, E.; Paszkowicz, W.; Guziewicz, M. Extremily low temperature growth of ZnO by atomic layer deposition. *J. Appl. Phys.* **2008**, *103*, No. 033515.
(47) Brundo, M. V.; Pecoraro, R.; Marino, F.; Salvaggio, A.; Tibullo, D.; Saccone, S.; Bramanti, V.; Buccheri, M. A.; Impellizzeri, G.; Scuderi, V.; Zimbone, M.; Privitera, V. Toxicity evaluation of new engineered nanomaterials in zebrafish. *Front Physiol.* **2016**, *7*, No. 130.
(48) Chen, W.-Y.; John, J. A.; Lin, C. H.; Lin, H. F.; Wu, S. C.; Lin, C. H.; Chang, C. Y. Expression of metallothionein gene during embryonic and early larval development in zebrafish. *Aquat. Toxicol.* **2004**, *69*, 215−227.

https://dx.doi.org/10.1021/acsabm.0c00409
ACS Appl. Bio Mater. 2020, 3, 4417−4426